Environmental Research 180 (2020) 108898

Contents lists available at ScienceDirect

Environmental Research

journal homepage: www.elsevier.com/locate/envres

Insights on adsorption of carbamazepine onto iron oxide modified diatomaceous earth: Kinetics, isotherms, thermodynamics, and mechanisms

Selly Jemutai-Kimosop[a], Francis Orata[a], Victor O. Shikuku[b,*], Veronica A. Okello[c], Zachary M. Getenga[c]

[a] Masinde Muliro University of Science and Technology, P.O.Box 190, Kakamega, Kenya
[b] Kaimosi Friends University College, P.O. Box 385-50309, Kaimosi, Kenya
[c] Machakos University, P.O.Box 136-90100, Machakos, Kenya

ARTICLE INFO

Keywords:
Diatomaceous earth
Carbamazepine
Adsorption
Non-linear regression

ABSTRACT

To ameliorate adsorbent recovery by an external magnetic field, naturally occurring diatomaceous earth (DE) was modified with iron-oxide, characterized and applied for adsorption of carbamazepine (CBZ) from synthetic wastewater using batch equilibration method. The fabricated adsorbent was characterized using XRF, XRD, SEM-EDX, FT-IR, BET surface area analysis, VSM and pH of point of zero charge (pH_{pzc}) determination. The adsorption rate was described by the pseudo-first-order (PFO) model suggesting a physisorption controlled rate-determining step. Equilibrium adsorption data were fitted to linear and nonlinear isotherm models, *viz* Langmuir and Freundlich models, and were best described by Freundlich nonlinear equations implying heterogeneous multilayer adsorption. The best-fitting kinetic and isotherm model was determined using four mathematical error functions. The thermodynamic parameters, namely enthalpy ($\Delta H = -26.4\ kJ\ mol^{-1}$), Gibbs free energy ($\Delta G = -2.22\ kJ\ mol^{-1}$ at 298 K), entropy ($\Delta S = -34.0\ kJ\ mol^{-1}$), indicated that the adsorption was a spontaneous, exothermic, and physical process. The adsorption mechanism is postulated to involve cation-π interactions. Modified diatomaceous earth is a potentially excellent, low-cost, and novel sorbent for CBZ adsorption with 88% removal in 180 min and provides a possible alternative adsorbent for wastewater treatment.

1. Introduction

Pharmaceuticals ingredients (PIs) are among the chemicals of emerging concern (CEC) also called emerging contaminants. Owing to their increased usage for human and veterinary disease control and treatment, pharmaceutical compounds and their metabolites find their way into the aquatic environments through the discharge of treated wastewater, seepage from landfills, septic systems, sewer lines and disposal of expired drugs into water systems among other pathways (Al-Hamadani et al., 2017). As a result, pharmaceuticals have been reported in a variety of environmental compartments including wastewater and drinking water (Jun et al., 2018; 2019). Studies have reported the accumulation of PIs in sewage sludge (Jelic et al., 2011), in surface waters (Davarnejad et al., 2018) and in public drinking water wells where septic systems are prevalent (Schaider et al., 2014). The occurrence of PIs in the aquatic environment has been linked with toxicity to aquatic organisms and inducing the development of drug-resistant bacterial strains making diseases difficult to treat (Azuma et al., 2019).

Carbamazepine, benzo[b][1]benzazepine-11-carboxamide, a human pharmaceutical for treating epileptic seizures, trigeminal neuralgia, bipolar depression, excited psychosis, and mania (Thacker, 2005) is not completely degraded in traditional wastewater treatment plants (WWTP) due to its recalcitrance to microbial biodegradation and removal efficiencies below 10% have been reported (Zhang et al., 2008). Sorption of carbamazepine onto sewage sludge is an ineffective sequestration pathway owing to its low affinity for organic matter (Kiecak et al., 2019). This explains the frequent occurrence of carbamazepine in WWTP effluents (Kimosop et al., 2016) at concentrations up to $10\ \mu g\ L^{-1}$ (Davarnejad et al., 2018).

A study by Oetken et al. (2005) demonstrated the toxicity of carbamazepine to aquatic insects. Furthermore, carbamazepine metabolites, such as aza-arenes, are potentially toxic and carcinogenic (Kosjek et al., 2009). Conventional wastewater treatment approaches for PIs removal include: adsorption (Bhadra and Jhung, 2017), biodegradation (Joss et al., 2006), membrane ultrafiltration (Heo et al., 2012), forward osmosis (Heo et al., 2013), and coagulation and flocculation (Boyd et al., 2003). However, adsorption of PIs from water remains the widely

* Corresponding author.
E-mail address: vshikuku@kafuco.ac.ke (V.O. Shikuku).

https://doi.org/10.1016/j.envres.2019.108898
Received 27 August 2019; Received in revised form 28 October 2019; Accepted 4 November 2019
Available online 07 November 2019
0013-9351/

used technique due to its relative low-price in capital investment, high removal efficiency, easy operation, and production of fewer toxic by-products (Bhadra and Jhung, 2017; Gao et al., 2018).

Several adsorbents have been fabricated and applied to ameliorate adsorption of PIs from wastewaters. These include activated carbon (Nam et al., 2014), iron modified clay (Shikuku et al., 2018a), modified biochars (Kimosop et al., 2017), ion-exchange resins (Jiang et al., 2015), graphene (Jauris et al., 2016), natural zeolites (Ng'eno et al., 2019), mesoporous silica (Bui et al., 2011), metal-organic frameworks (MOFs) (Jun et al., 2019) and diatomaceous earth (Tsai et al., 2006).

Diatomaceous earth (DE) is an amorphous naturally occurring material with unique physical and chemical properties such as high permeability and porosity, small particle size, high adsorption capabilities, low thermal conductivity and density, and high surface area of 10–30 $m^2 g^{-1}$ (Fields et al., 2003). Though diatomaceous earth has been reported for removal of bisphenol-A, a typical CEC, from water (Tsai et al., 2006), and for removal of other contaminants such as heavy metals (Hamadneh et al., 2019; Sosa et al., 2019) and dyes (Mohamed et al., 2019) with chemical modifications, there is scanty of information on removal of pharmaceutical compounds onto diatomaceous earth-based adsorbents. To the best of our knowledge, there is no published information on systematic adsorptive removal and adsorption mechanisms of carbamazepine (CBZ) onto modified diatomaceous earth (DE) under various environmental conditions. The presence of cavities in diatomaceous earth structure imbues DE with capabilities to trap pollutants and its natural occurrence makes it a low-cost adsorbent. The objectives of this work were to determine the adsorption efficiency of iron oxide modified diatomaceous earth (Fe-DE) for carbamazepine removal from synthetic wastewater, effects of solution pH, temperature and initial CBZ concentration and determine applicability of commonly used kinetic (pseudo-first and second-order) and isotherm (Langmuir and Freundlich) analysis using non-linear regression and evaluate the adsorption mechanism involved. Impregnation with Iron oxide improves the recovery of the exhausted pollutant-laden adsorbent *via* magnetic separation.

2. Materials and methods

2.1. Adsorbent preparation

The diatomaceous earth (DE), white in color, was obtained from Naivasha town in Kenya and was used to prepare the iron modified adsorbent (Fe-DE) without prior pre-treatment. Iron modified diatomaceous earth (Fe-DE) was prepared by direct hydrolysis of an iron salt as described by Hu et al. (2014) with slight modification. The iron salt solution was prepared by dissolving 10 g of $FeCl_3.4H_2O$ in 50 mL of deionized water and then mixed with 10 g of DE for 8 h under continuous agitation and finally filtered then oven-dried at 105 °C for 12 h. The resultant product, Fe-DE, was sieved to obtain uniform particle size (< 220 μm) then stored in air-tight containers for adsorption experiments.

2.2. Adsorbent characterization

The elemental composition of the unmodified diatomaceous earth (DE), and the iron-modified adsorbent (Fe-DE) were determined by XRF analysis. The specific surface area of Fe-DE was obtained by the BET liquid nitrogen adsorption-desorption method conducted at 77 K by employing a Micromeritics apparatus (Quadrasorb Evo 4, Quantachome, USA). The infrared spectrum of the untreated and modified DE samples was obtained using an ATR–FTIR spectrometer (Nicolet iS-5, USA) over the wavenumber range 4000–400 cm^{-1}. The crystalline phases and mineralogical composition were determined using an X-ray Brucker diffractometer (D8 Advance) with copper radiation (K_α = 1.5406). Surface morphology and elemental distribution were examined using a scanning electron microscope (SEM) (BITRI BSM 6460LV) coupled to an energy dispersive analysis X-ray (EDAX) instrument. The magnetic property of Fe-DE was measured using the DC SQUID magnetometer system (Magnetic Property Measurement System (MPSN) magnetometer model XL-5). The point of zero charge (pH_{pzc}) was determined using the pH drift method (Hosseinzadeh and Mohammadi, 2015).

2.3. Adsorption studies

Batch experiments were carried out in sealed 250-mL Erlenmeyer flasks where 0.1 g of Fe-DE was dispersed in 50 mL of 1 mg L^{-1} solution of carbamazepine (CBZ). The sealed flasks were agitated at 120 rpm in an overhead temperature controlled shaker at 298 K. At predetermined time intervals (0, 0.5, 1, 2, 3, 4, 5, 6 h), the residual CBZ in solution was determined. The effect of initial adsorbate concentration (0.25, 0.5, 0.75, 1.00 and 1.25 mg L^{-1}) at 298 K, and thermodynamic studies at 298, 308, 318, 328 and 338 K were evaluated, in triplicates, while holding other parameters constant. The effect of pH was studied in the range 2–10. The solution pH was modified using 0.1 M HCl and NaOH solutions. Aliquots of 0.5 mL were collected from the flasks at the predetermined equilibration time and sieved through 0.2-μm syringe filters into glass vials for analysis of the residual CBZ. Carbamazepine was analyzed by High-performance liquid chromatography (HPLC) with ultraviolet (UV) detection (Shimadzu LC 20AT) at 252 nm. The mobile phase was a mixture of acetonitrile and water (70:30 v/v), with a flow rate of 1 mL min^{-1}. The injection volume was 20 μL (Chen et al., 2016). The amount of solute adsorbed per unit mass of adsorbent at equilibrium (q_e) was calculated using the equation:

$$q_e = \frac{(C_i - C_e)V}{m} \quad (1)$$

Where V is the volume of solution (L), m is mass of adsorbent (g), C_i and C_e are the initial and equilibrium sorbate concentrations, respectively.

3. Results and discussion

3.1. Adsorbent characterization

3.1.1. Elemental composition

The elemental composition of the unmodified diatomaceous earth (DE), and the iron-modified adsorbent (Fe-DE) obtained by XRF analysis indicate successful impregnation of iron into the matrix (Table 1). The iron content increased from 15 to 71% following pre-treatment. The relative variation of the percent content of certain elements after chemical treatment suggests that iron inclusion involved cation exchange and or the metal ions leached into the solution. The Mn detected in Fe-DE could be previously shielded in DE sample or introduced as impurity in the iron salts.

Table 1
Elemental percent (%) composition of raw and treated diatomaceous earth.

	Fe	K	Ca	Si	Mn	Ti
DE	15.27 ± 0.95	3.20 ± 0.09	6.74 ± 0.89	73.45 ± 1.03	n.d	1.34 ± 0.07
Fe-DE	71.11 ± 1.02	1.42 ± 0.05	0.76 ± 0.02	26.44 ± 0.97	0.28 ± 0.10	n.d

*n.d-not detected.

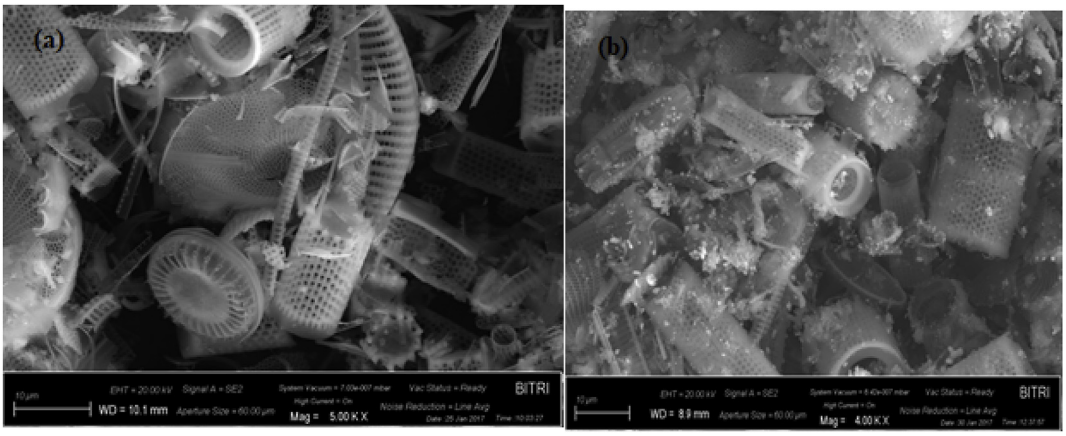

Fig. 1. SEM micrograph of (a) untreated diatomaceous earth (DE) (b) Fe-DE.

3.1.2. Surface morphology analysis

SEM micrographs of diatomaceous earth (DE) and the iron modified adsorbent (Fe-DE) are illustrated in Fig. 1 (a) and (b), respectively. The micrographs depict noticeable differences between the microstructures of the two materials with distinct micropores. The porous structure examination of the precursor DE depicts an assortment of rigid shapes and open cavities that imbue the diatomaceous earth with the capability to trap small-sized pollutant molecules (Yu et al., 2015). The textural features could be described as centroidal type frustules characterized by honeycomb structures. Chemical modification of DE resulted in flaws and small spherical-like iron oxide particle deposits shown in Fig. 1 (b) and the elemental distribution of iron in Fe-DE depicted in the SEM-EDX micrograph in Fig. 2.

3.1.3. Crystallinity and mineralogical analysis

The untreated diatomaceous earth was notably rich in amorphous SiO_2 forms with no detectable crystalline phases noted (Fig. 3). However, after chemical treatment, crystallinity was induced and the crystallized iron phase incorporated as shown in the diffractogram (Fig. 4) was hematite (α-Fe_2O_3). The strong and sharp reflection XRD peaks were observed at 2Θ values of 24.07°(012), 33.09°(104), 35.53°(110), 40.67°(113), 49.39°(024), 53.91°(116), 57.45°(022), 62.35°(214) and 63.86°(300) (Fig. 4) suggesting that the synthesized Fe-DE composite was well crystallized with rhombohedral structure (Knoerr et al., 2013).

3.1.4. Functional group analysis

The FTIR spectra of the diatomaceous earth (DE) and its iron modified counterpart (Fe-DE) are displayed in Fig. 5. There was a significant reduction in band intensities and width for all major characteristic bands which would bear implication quantitatively. Qualitatively, there was no appreciable new peak suggesting no new functional group added after pre-treatment. A similar phenomenon has been reported in other studies (Shikuku et al., 2018a). The wavebands ranging from 1200 to 1000 and 795 cm^{-1}) were due to silicates structure (Fujiwara et al., 2006). The wide bands centered at around 1090 cm^{-1} were attributed to Si–O–Si in-plane vibration (asymmetric stretching). Similar observations can be seen at 795 cm^{-1}, which are also characteristic of silica. Again, the weak absorption band at 616 cm^{-1} was possibly attributed to Si–O deformation and Al–O stretching (Yuan et al., 2013). The broad absorption band at 3600–3700 cm^{-1} corresponds to the structural –OH stretching vibration and probably outer –OH groups from surface adsorbed water (Namduri and Nasrazadani, 2008).

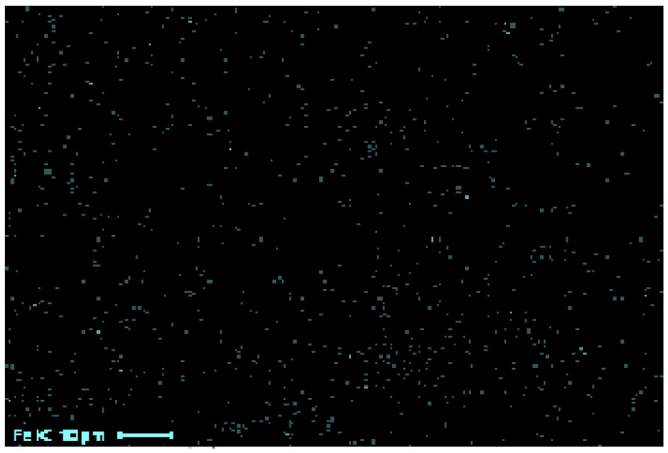

Fig. 2. SEM-EDAX micrograph showing the iron distribution in Fe-DE.

3.1.5. Surface area analysis

The surface area of Fe-DE was determined by Brunauer–Emmet–Teller (BET) method and the total pore volume and the average pore diameter derived from the Barrett–Joyner–Halenda (BJH) method. The BET surface area for Fe-DE was 22.0 $m^2 g^{-1}$ with a BJH desorption surface area of 20.5 $m^2 g^{-1}$. The total pore volume was 0.0609 $cm^3 g^{-1}$ and an average pore diameter of 11.9 nm.

3.1.6. Magnetic properties

To understand the magnetic properties of the Fe-DE adsorbent, a magnetic hysteresis curve, obtained using a vibrating sample magnetometer (VSM), was recorded at a temperature range between 0 and 350 K at a constant magnetic field of 1000 Oe. The fabricated Fe-DE ferromagnetic properties are shown in Fig. 6. This property is essentially important for the convenient recovery of contaminant-laden adsorbent from a continuously flowing system using an external magnetic field (Zhang et al., 2013). Notably, Fe-DE exhibited ferromagnetic behavior at low temperature changing to paramagnetic above 25 K.

3.2. Effect of contact time and adsorption kinetics

The percent removal (%R) of carbamazepine (CBZ) by the iron modified diatomaceous earth (Fe-DE) as a function of time depicted fast adsorption kinetics leading to saturation within 180 min (Fig. 7) depicted by a plateau equilibrium phase with no change in amount adsorbed. A maximum percent removal (%R) of 88% CBZ was achieved at equilibrium. The initial high removal extent is due to the availability of a large number of vacant adsorption sites. However, accessibility to these sites becomes progressively limited following occupancy by the CBZ molecules and repulsion between the adsorbed molecules and those in the bulk solution resulting in equilibrium. Shorter equilibrium times are desirable for real wastewater treatment for they imply

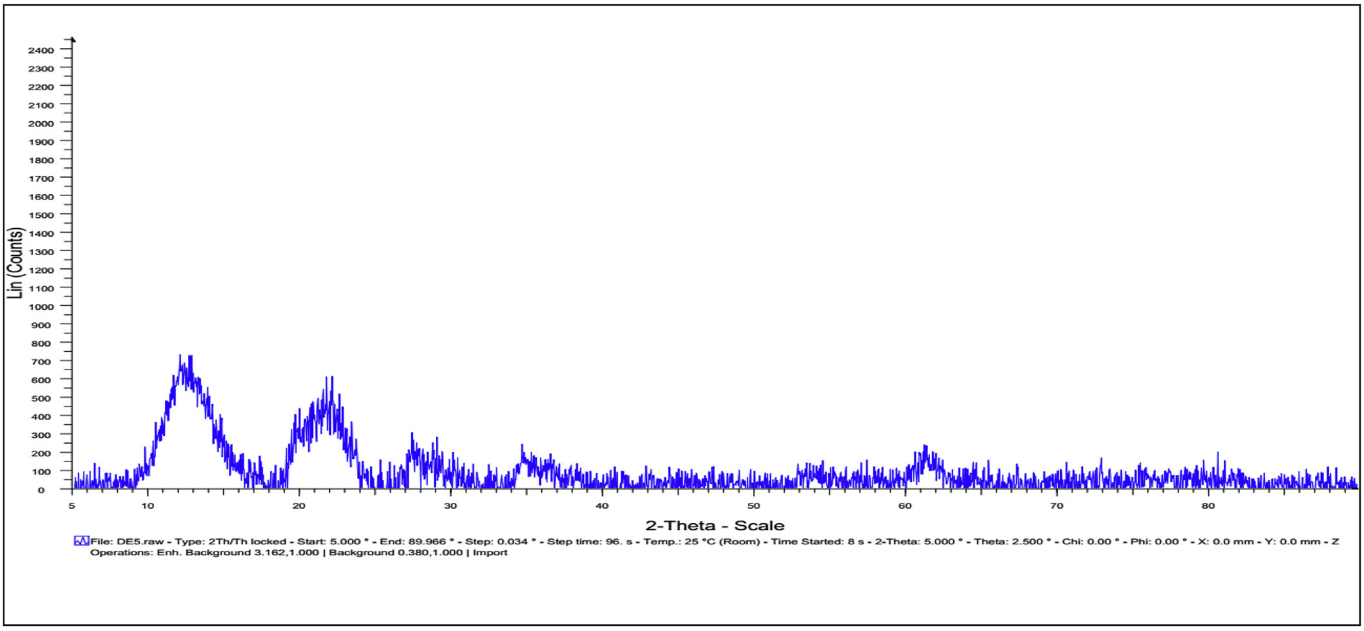

Fig. 3. The XRD pattern for unmodified diatomaceous earth (DE) adsorbent.

reduced residence time.

To gain insight on the adsorption rate and nature of the rate-controlling step(s), the kinetic data were simulated using pseudo-first-order (PFO) (Ho and McKay, 1998) and pseudo-second-order (PSO) (Ho, 2006) kinetic models. The suitability of the model was evaluated by non-linear coefficient of determination (R^2) values, four error functions, namely; Hybrid fractional error function (HYBRID), Marquart's percentage standard deviation (MPSD), Sum of squares error (SSE) and Average relative error (ARE) and the degree of agreement between experimental equilibrium adsorption capacity (q_{exp}) and the theoretical values (q_{cal}) predicted by the models. The error function equations are shown in Table 2 and the calculated values for the non-linear kinetic models' parameters are listed in Table 3.

$$\text{Pseudo} - \text{first} - \text{order (PFO) model: } q_t = q_e\left(1 - e^{-k_1 t}\right) \quad (2)$$

$$\text{Pseudo} - \text{second} - \text{order (PSO) model: } q_t = \frac{q_e^2 k_2 t}{1 + k_2 q_e t} \quad (3)$$

The pseudo-first-order (PFO) model revealed a perfect fitting to the experimental data with R^2 value of unity, low error function values compared to PSO and a match between the model predicted (q_{cal}) and experimental (q_{exp}) adsorption capacities. Though, the pseudo-second-order (FSO) kinetic model revealed equally high R^2 value (0.997), the relatively wider variance between the calculated and experimental

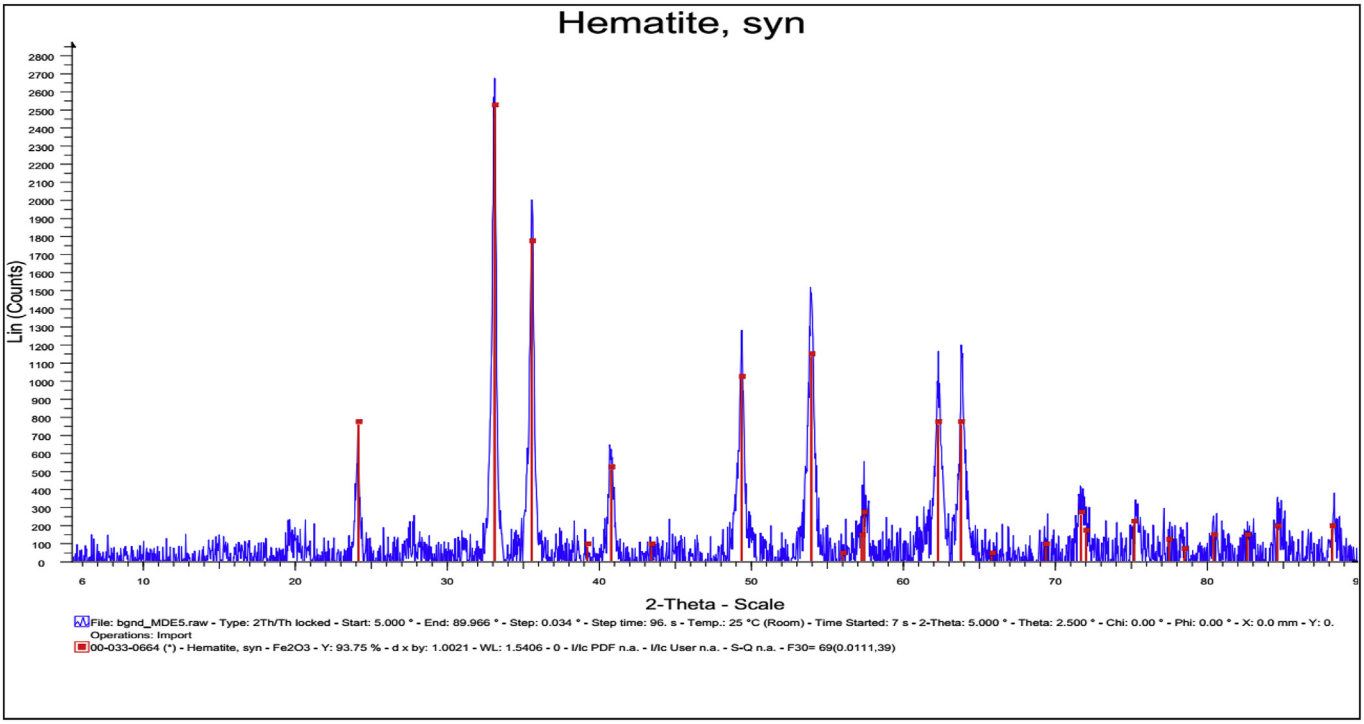

Fig. 4. The XRD pattern for iron modified diatomaceous earth (Fe-DE).

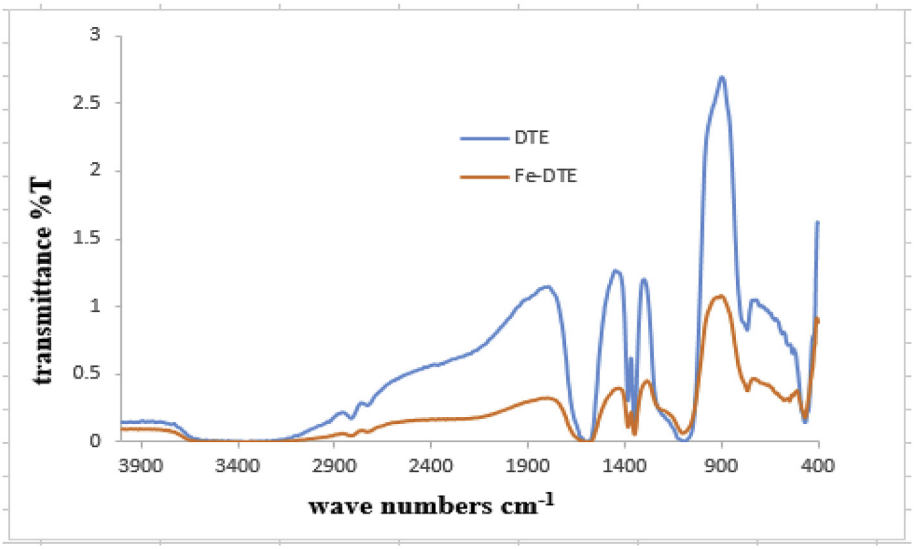

Fig. 5. FTIR spectra of natural and modified diatomaceous earth.

equilibrium capacities and the notably high HYBRID, MPSD and ARE values denote that the adsorption of CBZ onto the Fe-DE is not a PSO reaction. Conformity to the PFO kinetics implies the rate-controlling step is a physisorption process and does not involve the exchange of valence electrons.

3.3. Isotherm modeling

3.3.1. Langmuir isotherm

Langmuir (1916) derived an empirical model hypothesizing monolayer adsorption of molecules onto a morphologically homogeneous adsorbent surface with a fixed number of active adsorption sites without lateral interactions. The model postulates that all the binding sites are energetically identical. Langmuir further postulated that the intermolecular attractive interactions decrease steadily with increased distance. The original non-linear form of the Langmuir equation is expressed as:

$$q_e = \frac{Q_0 K_L C_e}{1 + K_L C_e} \quad (4)$$

Where q_e is the amount of adsorbate adsorbed per unit mass of the sorbent at equilibrium (mg g^{-1}), C_e is the residual adsorbate concentration in the solution at equilibrium (mg L^{-1}), Q_o is the maximum adsorption density (mg g^{-1}) and K_L is the Langmuir constant related to the free energy of adsorption (L g^{-1}). The Lineweaver-Burk linearization of the Langmuir equation is shown in Table 4.

3.3.2. Freundlich isotherm

The Freundlich (1906) model predicts a multilayer adsorption process, with non-uniform distribution of adsorption energies onto the heterogeneous adsorbent surface without lateral interaction. The model postulates occupancy of the energetically favored binding sites first as the binding strength diminishes sequentially with increased coverage of the adsorbing sites. The non-linear Freundlich equation is expressed as:

$$q_e = K_F C_e^{1/n} \quad (5)$$

The linearized form of the equation is presented in Table 4.

The conformity of the equilibrium data to the two mathematical models was examined and their applicability tested using both linear and non-linear regression analysis approaches. The linearized isotherm model parameter values are listed in Table 5 and those calculated from the non-linear form are presented in Table 6.

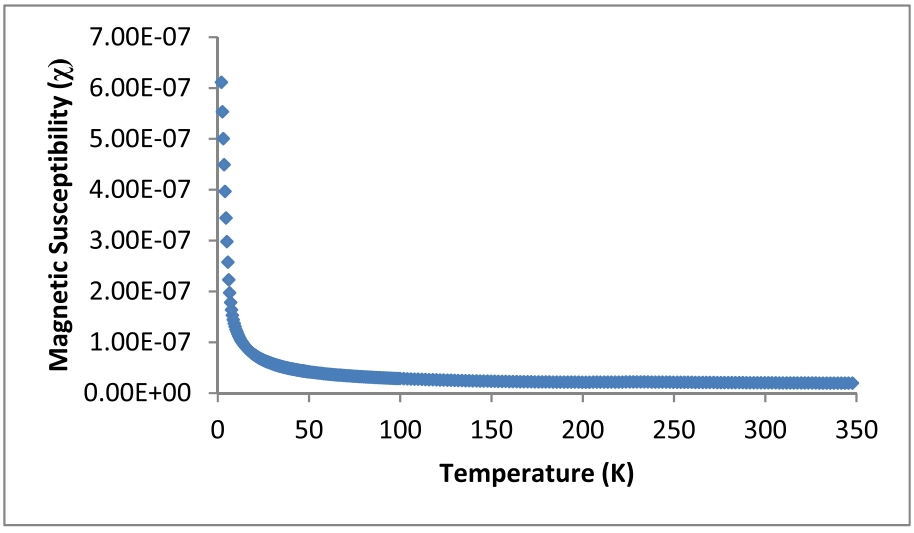

Fig. 6. Magnetic hysteresis loop for Fe-DE adsorbent.

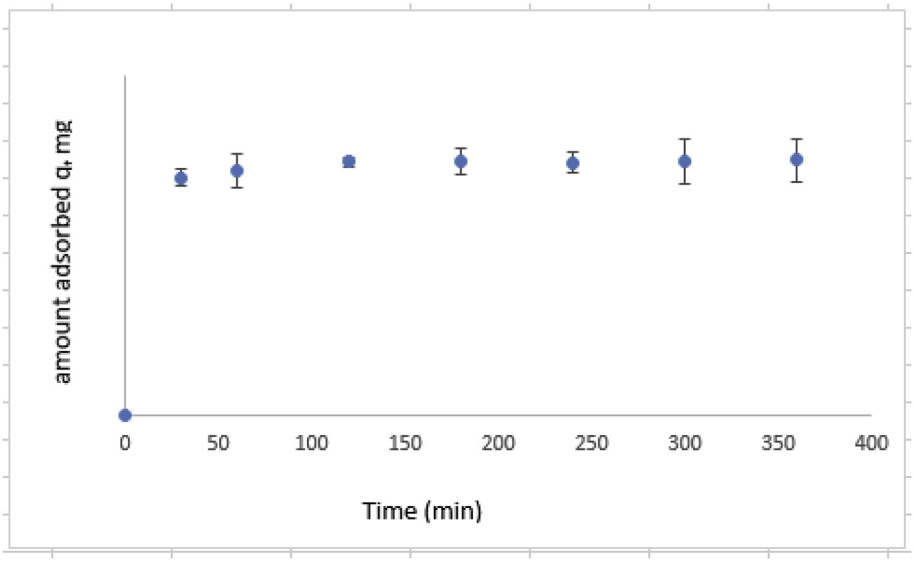

Fig. 7. Variation of percent removal of CBZ by Fe-DE with time.

3.3.3. Langmuir isotherm analysis

The two equations, Lineweaver-Burk linearization of the Langmuir model and the original non-linear Langmuir equation had not only varying coefficients of determination but also widely dissimilar Langmuir parameters (see Tables 5 and 6). This shows that the linearization of non-linear functions induces errors that may undermine the theoretical basis of the model (Shikuku et al., 2018a). The theoretical Langmuir monolayer (Q_o) maximum adsorption density parameter varied by a factor of 22 a testament that Lineweaver-Burk linearization of Langmuir equation, though extensively used, overestimated the adsorption capacity of the sorbent. This variance indicates that the linearization of adsorption isotherms should be discouraged as it may lead to errors in parameter estimations, interpretations and conclusions (Ng'eno et al., 2019; Shikuku et al., 2018b). Langmuir isotherm is also described in terms of the dimensionless parameter called the separation factor (R_L) [47] expressed as:

$$R_L = \frac{1}{1 + K_L C_o} \tag{6}$$

In this work, the separation constant (R_L) values are below unity denoting the adsorption process was not favorable (Hall et al., 1966). However, despite on the aforementioned discrepancies, the coefficient of determination value favored the linear Langmuir isotherms.

3.3.4. Freundlich isotherm analysis

The data were further modeled using the linearized and non-linear expressions of the Freundlich equation and the constants are listed in Tables 5 and 6. Here, it is also noteworthy that the linearization of the Freundlich equation significantly underestimated the Freundlich constant (K_F) by a magnitude of 10. This puts to question the validity of most conclusions in literature derived from linearized isotherms. Traditionally, the coefficient of determination (R^2) has been used to determine the best-fit isotherm for both linear and non-linear models.

Table 3
The kinetic model parameters for CBZ adsorption onto Fe-DE.

Kinetic model	PFO	PSO
Parameters	$q_{e(cal)}$ mg g^{-1} = 0.442 K_1 min^{-1} = 55537.2 $q_{e(exp)}$ mg g^{-1} = 0.442	$q_{e(cal)}$ mg g^{-1} = 0.689 K_2 g $mg^{-1}min^{-1}$ = 0.0015 $q_{e(exp)}$ mg g^{-1} = 0.442
R^2	1.000	0.997
HYBRID	0.06	27.32
MPSD	2.49	52.27
SSE	0.001	0.35
ARE	2.92	61.72

Table 4
Linearized isotherm equations and model parameters.

Isotherm Model	Equation	Parameters	plot
Langmuir-1	$\frac{1}{q_e} = \frac{1}{Q_o} + \frac{1}{Q_o K_L C_e}$	Q_o (mg g^{-1}) K_L (L g^{-1})	$\frac{1}{q_e} vs \frac{1}{C_e}$
Freundlich	$\ln q_e = \ln K_f + \frac{1}{n} \ln C_e$	K_f, n	$\ln q_e vs \ln C_e$

Table 2
Mathematical error functions for testing the best-fit isotherm model.

Error function	Equation	Definition of parameters
Hybrid fractional error function (HYBRID)	$\frac{100}{n-p}\sum_{i=1}^{n}\frac{\left(q_{e(\exp)} - q_{e(cal)}\right)^2}{q_{e(\exp)}}$	$q_{e(exp)}$: experimental values
Marquart's percentage standard deviation (MPSD)	$100\left(\sqrt{\frac{1}{n-p}\sum_{i=1}^{n}\frac{\left(q_{e(\exp)} - q_{e(cal)}\right)^2}{q_{e(\exp)}}}\right)$	$q_{e(cal)}$: calculated values
Sum of squares error (SSE)	$\sum_{i=1}^{n}(q_{e(cal)} - q_{e(\exp)})^2$	n: the number of data points in the experimental data;
Average relative error (ARE)	$\frac{100}{n}\sum_{i=1}^{n}\frac{\left(q_{e(\exp)} - q_{e(cal)}\right)}{q_{e(\exp)}}$	p: the number of parameters in the isotherm model.

Table 5
Linear Langmuir and Freundlich isotherm model parameters for CBZ adsorption.

Isotherm model	Parameters		R^2
Linear Langmuir	Q_0 mg g^{-1}	0.447	0.796
	K_L L g^{-1}	7.050	
	R_L	0.102	
Linear Freundlich	1/n	0.694	0.720
	K_F (L g^{-1})	0.853	

Table 6
Non-linear Langmuir and Freundlich isotherm model parameters for CBZ adsorption.

Isotherm model	Non-linear Langmuir	Non-linear Freundlich
Parameters	Q_0 mg g^{-1} = 0.019	K_F (L mg^{-1}) = 9.125
	K_L L g^{-1} = 1.819	1/n = 2.289
	R_L = 0.305	
R^2	0.600	0.800
HYBRID	4.59	4.16
MPSD	21.40	20.30
SSE	0.04	0.02
ARE	29.17	30.23

However, R^2 has been reported to be an inadequate tool as the sole criterion for the determination of goodness of fit (Zheng et al., 2019). Similarly, to determine the best fitting isotherm to describe the empirical data, the four mathematical error functions (HYBRID, MPSD, SSE and ARE) were used. The low R^2 and relatively higher error function values imply the postulates of the Langmuir model could not satisfactorily describe the adsorption process. Similar findings have been reported for CBZ adsorption onto hematite nanoparticles (Rajendran and Sen, 2018). Based on the error functions, the Freundlich model best fitted the experimental data relative to the Langmuir isotherm suggesting multilayer adsorption. According to Treybal (1981), the magnitude of n is related to the favorability of the adsorption process. Treybal notes that n values in the range 2–10 represent good, 1–2 moderately difficult, and less than 1 a poor adsorptive potential. In the present work, the magnitude of n (0.436) indicates a poor adsorption process. Smaller values of 1/n depict the formation of relatively strong bonds between the adsorbate molecules and adsorbent (To et al., 2017). The 1/n value observed (Table 4), implies weaker adsorbate-adsorbent interactions suggesting a physical adsorption process. Furthermore, the $1/n$ values above unity, as in this study, suggest cooperative adsorption involving multi-mechanistic adsorption sequences (Saleh, 2015).

Giles et al. (1974) classified isotherms for adsorption of organic solutes into four main groups: L, S, H, and C and thereafter into subgroups. Based on this classification, the isotherm of CBZ displayed an S-type curve structure (Fig. 8). Conformity to the S-shaped adsorption isotherm implies there is strong competition between CBZ and the water (solvent) molecules for the adsorption sites. The rising curve structure without a plateau implies that the orientation of the adsorbed CBZ molecules generates new adsorption areas with relatively high affinity for more CBZ molecules, corroborating the cooperative adsorption alluded to by the Freundlich function 1/n.

3.4. Effect of pH and adsorption mechanism

The effect of pH on adsorption of carbamazepine (CBZ) onto the iron oxide modified diatomaceous earth was studied in the range pH 2–10 and the percent removal (%R) as a function of pH is depicted in Fig. 9.

CBZ adsorption was practically unaffected by pH variation with percent removal ranging between 87.2 and 88.8% in the pH range. This phenomenon could be explained by comparing the pH_{pzc} of the adsorbent (6.0) (Fig. 10) and the pK_a values of carbamazepine. In principle, the adsorbent surface charge is expected to bear net positive charge at pH below 6 and negatively charged above pH of point of zero charge.

Furthermore, from FTIR analysis, the adsorbent showed characteristic bands of hydroxyl groups (-OH; pK_a 9.5–13) (Volesky, 2007). Therefore, in the pH range of the study (2–10), these –OH groups were protonated and the surface chemistry of adsorbent could be expressed as:

$$Fe - DE - OH \leftrightarrow Fe - DE - OH_2^+ \quad (7)$$

On the other hand, CBZ is characterized by two pK_a values; pK_{a1} at 2.30 (ketone group) and pK_{a2} 13.90 (amine group) (Punyapalakul and Sitthisorn, 2010). Therefore, with $pK_{a1} < 2.3$ and $pK_{a2} \geq 13.9$, CBZ existed completely as a neutral species (CBZ^0) in the pH range, 2–10, of the study. As such, electrostatic attractions were insignificant and therefore ruled out as the adsorption mechanism. This is also evidenced by the independence of the percent removal (%R) on solution pH and corroborated by similar findings (Mahramanlioglu and Onnar, 2013;

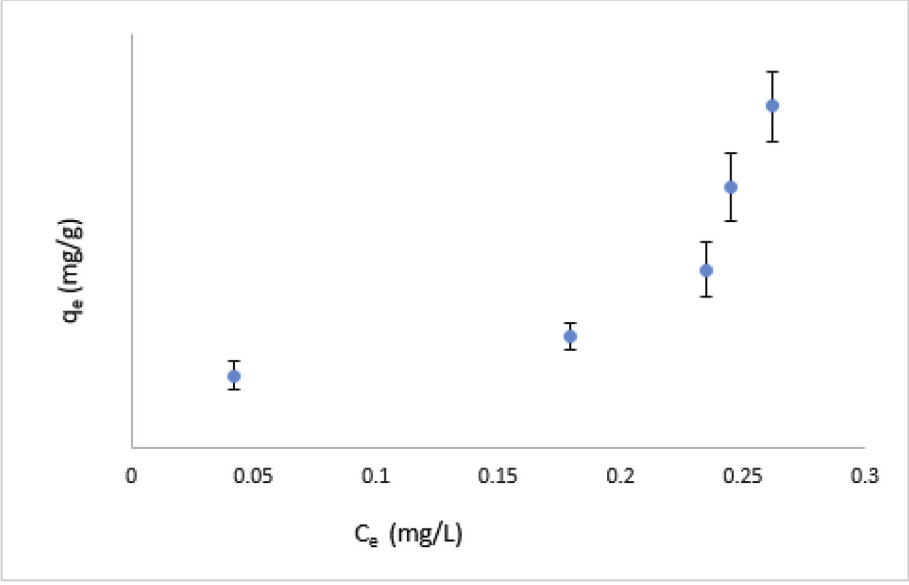

Fig. 8. Experimental adsorption isotherm for CBZ removal onto Fe-DE.

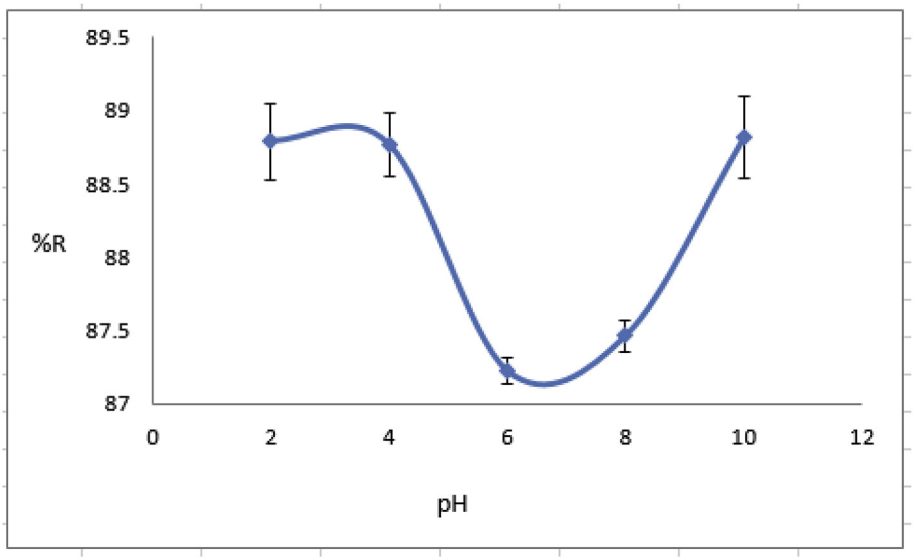

Fig. 9. Variation of the amount of CBZ adsorbed onto Fe-DE as a function of pH.

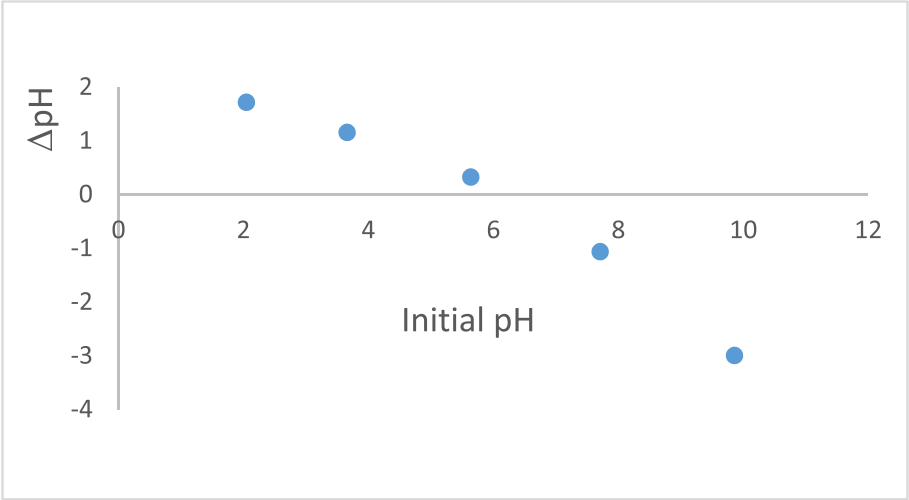

Fig. 10. Point of zero charge plot for Fe-DE.

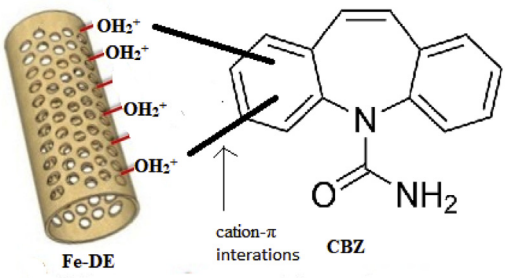

Fig. 11. Adsorption mechanism of CBZ onto Fe-DE at pH 2-10.

Rajendran and Sen, 2018). Therefore, non-electrostatic interactions are necessarily involved. Cation-π interactions between the positively charged adsorbent surface ($Fe-DE-OH_2^+$) and the π-system of the CBZ molecule is proposed as a possible adsorption mechanism (Fig. 11) (Zhao et al., 2017). Furthermore, the cooperative adsorption denoted by the Freundlich function 1/n may also imply π-π interactions/ stacking.

Table 7
Thermodynamic parameters for CBZ adsorption onto Fe-DE.

Compound	Temp.(K)	% removal	ΔG (KJ mol^{-1})	ΔH (kJ mol^{-1})	ΔS (kJ mol^{-1})
CBZ	298	90.15	−2220	−26.40	−34.04
	308	88.90	−1304		
	318	74.52	−1290		
	328	67.45	−1071		
	338	55.40	−873		

3.5. Adsorption thermodynamics

The effect of temperature was studied in between 298 and 338 K. The thermodynamic functions, changes in Gibb's free energy (ΔG), enthalpy (ΔH) and entropy (ΔS), related to the adsorption processes were calculated from the equations below and the results are summarized in Table 7:

$$\Delta G = -RT \ln K_c \quad (8)$$

$$K_c = \frac{C_{ads}}{C_e} \quad (9)$$

Table 8
Comparison of Fe-DE performance with other adsorbents.

Adsorbent	Adsorption capacity (mg g^{-1})	Contact time	% Removal	Reference
Magnetite-modified magnetic carbon nanotubes	0.065	3 h	80	Deng et al. (2019)
Hematite nanoparticles	2.890	2.5 h	55	Rajendran and Sen, 2018
Pinewood derived nanobiochar	0.116	3 h	70–99	Naghdi et al. (2017)
Magnetic activated carbon	182.9	–	93	Baghdadi et al. (2016)
Magnetic bagasse derived biochar	–	4 h	60.9	Kimosop et al. (2017)
Nucifera extract-coated magnetic nanoparticle	0.715	3 h	51.4	Misra et al. (2018)
Expanded graphite	43.54	1.5 h	70	Borisova et al. (2013)
Fe-DE	–	2 h	88.2	This study

$$\ln K_c = \frac{\Delta S}{R} - \frac{\Delta H}{R}\frac{1}{T} \quad (10)$$

Where K_c is the equilibrium constant, C_e is the equilibrium concentration in the solution (mg L^{-1}) and C_{ads} is the equilibrium solid phase concentration (mg g^{-1}). R is the gas constant (8.314 J $mol^{-1}K^{-1}$) and T is the temperature (K).

From Table 7, the percent (%) removal of CBZ consistently decreased with rising temperature indicating an exothermic process and is confirmed by the negative ΔH value. This decrease is attributable to the increased water solubility of the adsorbate at higher temperatures with the concomitant weakening of the adsorbate affinity for the adsorbent surface (Shikuku et al., 2018a).

The negative ΔG values imply the adsorption of CBZ onto Fe-DE is a spontaneous process. Nevertheless, the reaction becomes less favorable with increased temperature due to its exothermicity. The ΔH value (26.40 kJ mol^{-1}), far below 40 kJ mol^{-1}, indicates that the adsorption mechanism of CBZ onto Fe-DE is physical in nature (Shikuku et al., 2015) consistent with both the PFO model and the proposed cation-π interactions.

4. Comparison with other adsorbents

The performance of Fe-DE for removal of CBZ was compared with other adsorbents in literature in terms of Langmuir maximum adsorption capacities, percent removal (%R) and contact time and the comparison data presented in Table 8. It can be seen that Fe-DE is an efficient low-cost adsorbent for CBZ removal relative to other reported materials.

5. Conclusion

In this work, naturally occurring diatomaceous earth (DE) was chemically modified with iron to improve adsorbent recovery by an external magnetic field. The product (Fe-DE) was used for adsorption of carbamazepine (CBZ) from synthetic wastewater. Fe-DE showed a higher adsorption efficiency of 88.2% with equilibration at 180 min. Best fitting kinetics and isotherm models were determined by error analysis using four mathematical error functions. The equilibrium adsorption data were described by the nonlinear Freundlich isotherm model suggesting multilinear adsorption. Linearization of adsorption isotherms is shown to significantly underestimate or overestimate the calculated isotherm parameters. Adsorption kinetics followed pseudo-first-order (PFO) kinetics while thermodynamics investigation revealed the adsorption process to be spontaneous and exothermic. The magnitude of ΔH, 1/n, and conformity to PFO indicated that the adsorption mechanism was physical in nature. Cation-π interactions are proposed as the possible driving adsorption mechanism of CBZ onto Fe-DE though other possibilities such as hydrophobic and π-π stacking may play a role.

Funding

This work was supported by the International Foundation for Science (IFS), grant number W/5587-1.

Appendix A. Supplementary data

Supplementary data to this article can be found online at https://doi.org/10.1016/j.envres.2019.108898.

References

Al-Hamadani, Y.A.J., Park, C.M., Assi, L.N., Chu, K.H., Hoque, S., Jang, M., Yoon, Y., Ziehl, P., 2017. Sonocatalytic removal of ibuprofen and sulfamethoxazole in the presence of different fly ash sources. Ultrason. Sonochem. 39, 354–362.

Azuma, T., Kana, O., Shiori, M., Mao, I., Kanae, H., Ayami, Y., Yoshiki, M., Tetsuya, H., 2019. Environmental fate of pharmaceutical compounds and antimicrobial-resistant bacteria in hospital effluents, and contributions to pollutant loads in the surface waters in Japan. Sci. Total Environ. 657, 476–484. https://doi.org/10.1016/j.scitotenv.2018.11.433.

Baghdadi, M., Ghaffari, E., Aminzadeh, B., 2016. Removal of carbamazepine from municipal wastewater effluent using optimally synthesized magnetic activated carbon: adsorption and sedimentation kinetic studies. J. Environ. Chem. Eng. 4 (3), 3309–3321.

Bhadra, B.N., Jhung, S.H., 2017. A remarkable adsorbent for removal of contaminants of emerging concern from water: porous carbon derived from metal azolate framework-6. J. Hazard Mater. 340, 179–188.

Borisova, D.A., Vedenyapina, M.D., Strel'tsova, E.D., Maslov, V.L., Rosenwinkel, K.H., Weichgrebe, D., Stopp, P., Vedenyapin, A.A., 2013. Adsorption of carbamazepine from aqueous solutions on expanded graphite. Solid Fuel Chem. 47, 298. https://doi.org/10.3103/S0361521913050030.

Boyd, G.R., Reemtsma, H., Grimm, D.A., Mitra, S., 2003. Pharmaceuticals and personal care products (PPCPs) in surface and treated waters of Louisiana, USA and Ontario. Canada. Sci. Total Environ. 311, 135–149.

Bui, T.X., Kang, S.Y., Lee, S.H., Choi, H., 2011. Organically functionalized mesoporous SBA-15 as sorbents for removal of selected pharmaceuticals from water. J. Hazard Mater. 193, 156–163.

Chen, J., Zhang, D., Zhang, H., Ghosh, S., Pan, B., 2016. Fast and slow adsorption of carbamazepine on biochar as affected by carbon structure and mineral composition. Sci. Total Environ. https://doi.org/10.1016/j.scitotenv.2016.11.052.

Davarnejad, R., Soofi, B., Farghadani, F., Behfar, R., 2018. Ibuprofen removal from a medicinal effluent: a review on the various techniques for medicinal effluents treatment. Environ. Technol. Innov. 11, 308–320.

Deng, Y., Ok, Y., Mohan, D., Pittman, C., Dou, X., 2019. Carbamazepine removal from water by carbon dot-modified carbon nanotubes. Environ. Res. 169, 434–444.

Fields, S., Korunic, Z., McLaughlin, A., Stathers, T., 2003. Standardized testing for diatomaceous earth. In: Proceedings of the 8th International Conference on Stored-Product Protection, pp. 779–784.

Freundlich, H.M.F., 1906. Ü ber die adsorption in lösungen. Z. Phys. Chem. 57, 385–470.

Fujiwara, M., Shiokawa, K., Sakakura, I., Nakahara, Y., 2006. Silica hollow spheres with nano-macroholes like diatomaceous earth. Chemosphere 33, 3–6.

Gao, Y., Liu, K., Kang, R., Xia, J., Yu, G., Deng, S., 2018. A comparative study of rigid and flexible MOFs for the adsorption of pharmaceuticals: kinetics, isotherms and mechanisms. J. Hazard Mater. 359, 248–257.

Giles, C., D'Silva, A.P., Easton, I.A., 1974. A general treatment and classification of the solute adsorption isotherm. I. Theor. J. Colloid Interface Sci. 47, 766.

Hall, K.R., Eagleton, L.C., Acrivos, A., Vermeulen, T., 1966. Pore and solid-diffusion kinetics in fixed–bed adsorption under constant–pattern conditions. Ind. Eng. Chem. Fundam. 5, 212–223.

Hamadneh, I., Alatawi, A., Zalloum, R., Albuqain, R., Alsotari, S., Khalili, F.I., Al-Dujaili, A.H., 2019. Comparison of Jordanian and standard diatomaceous earth as an adsorbent for removal of Sm(III) and Nd(III) from aqueous solution. Environ. Sci. Pollut. Res. 26, 20969–20980.

Heo, J., Boateng, L.K., Flora, J.R.V., Lee, H., Her, N., Park, Y.G., Yoon, Y., 2013. Comparison of flux behavior and synthetic organic compound removal by forward osmosis and reverse osmosis membranes. J. Membr. Sci. 443, 69–82.

Heo, J., Flora, J.R.V., Her, N., Park, Y.G., Cho, J., Son, A., Yoon, Y., 2012. Removal of bisphenol A and 17 b-estradiol in single walled carbon nanotubes-ultrafiltration (SWNTs-UF) membrane systems. Separ. Purif. Technol. 90, 39–52.

Ho, Y.S., 2006. Review of second-order models for adsorption systems. J. Hazard Mater.

136, 681–689.
Ho, Y.S., McKay, G., 1998. Sorption of dye from aqueous solution by peat. Chem. Eng. J. 70, 115–124.
Hosseinzadeh, H., Mohammadi, S., 2015. Quince seed mucilage magnetic nanocomposites as novel bioadsorbents for efficient removal of cationic dyes from aqueous solutions. Carbohydr. Polym. 134, 213–221.
Hu, X., Ding, Z., Zimmerman, A.R., Wang, S., Gao, B., 2014. Batch and column sorption of arsenic onto iron-impregnated biochar synthesized through hydrolysis. Water Res. 68, 206–216.
Jauris, I.M., Matos, C.F., Saucier, C., Lima, E.C., Zarbin, A.J.G., Fagan, S.B., Machado, F.M., Zanella, I., 2016. Adsorption of sodium diclofenac on graphene: a combined experimental and theoretical study. Phys. Chem. Chem. Phys. 18, 1526–1536.
Jelic, A., Gros, M., Ginebreda, A., Cespedes-Sánchez, R., Ventura, F., Petrovic, M., Barceló, D., 2011. Occurrence, partition and removal of pharmaceuticals in sewage water and sludge during wastewater treatment. Water Res. 45, 1165–1176.
Jiang, M., Yang, W., Zhang, Z., Yang, Z., Wang, Y., 2015. Adsorption of three pharmaceuticals on two magnetic ion-exchange resins. J. Environ. Sci. Technol. 31, 226–234.
Joss, A., Zabczynski, S., G€obel, A., Hoffmann, B., L€offler, D., McArdell, C.S., Ternes, T.A., Thomsen, A., Siegrist, H., 2006. Biological degradation of pharmaceuticals in municipal wastewater treatment: proposing a classification scheme. Water Res. 40, 1686–1696.
Jun, B.M., Kim, S., Heo, J., Her, N., Jang, M., Park, C.M., Yoon, Y., 2019. Enhanced sonocatalytic degradation of carbamazepine and salicylic acid using a metal organic framework. Ultrason. Sonochem. 56, 174–182.
Jun, B.M., Lee, H.K., Kwon, Y.N., 2018. Acid-catalyzed hydrolysis of semi-aromatic polyamide NF membrane and its application to water softening and antibiotics enrichment. Chem. Eng. J. 332, 419–430.
Kiecak, A., Lara, S., Mercè, B., Elsner, M., Mas-Pla, J., Salle, C., Stumpp, C., 2019. Sorption properties and behaviour at laboratory scale of selected pharmaceuticals using batch experiments. J. Contam. Hydrol. 225, 103500.
Kimosop, S.J., Getenga, Z.M., Orata, F.O., Okello, V.A., Cheruiyot, J.K., 2016. Residue levels and discharge loads of antibiotics in wastewater treatment plants and hospital lagoons within Lake Victoria Basin, Kenya. J. Environ. Monit. Assess. 188, 532. https://doi.org/10.1007/s10661-016-5534-6.
Kimosop, S.J., Okello, V.O., Orata, F., Getenga, Z.M., Shikuku, V.O., 2017. Green Remediation of carbamazepine from water using iron modified carbonized bagasse: kinetics, equilibrium and mechanistic studies. Chem. Sci. Inter. J. 18 (3), 1–9.
Knoerr, R., Brendlé, J., Lebeau, B., Demais, H., 2013. Microporous and Mesoporous Materials Preparation of ferric oxide modified diatomite and its application in the remediation of as (III) species from solution. Microporous Mesoporous Mater. 169, 185–191. https://doi.org/10.1016/j.micromeso.2012.09.036.
Kosjek, T., Andersen, H.R., Kompare, B., Ledin, A., 2009. Fate of carbamazepine during water treatment. Environ. Sci. Technol. 43, 6256–6261.
Langmuir, I., 1916. The constitution and fundamental properties of solids and liquids. J. Am. Chem. Soc. 38, 2221–2295.
Mahramanlioglu, M., Onnar, O.O., 2013. Adsorption of carbamazepine on the adsorbent produced from spent bleaching earth. Asian J. Chem. 25, 1033–1035.
Misra, T., Mitra, S., Sen, S., 2018. Adsorption studies of carbamazepine by green-synthesized magnetic nanosorbents. Nanotechnol. Environ. Eng. 3. https://doi.org/10.1007/s41204-018-0040-4.
Mohamed, E.A., Selim, A.Q., Zayed, A.M., Komarneni, S., Mobarak, M., Seliem, M.K., 2019. Enhancing adsorption capacity of Egyptian diatomaceous earth by thermochemical purification: methylene blue uptake. J. Colloid Interface Sci. 534, 408–419.
Naghdi, M., Taheran, M., Pulicharla, R., Rouissi, T., Brar, S., Verma, M., Surampalli, R.Y., 2017. Pine-wood derived nanobiochar for removal of carbamazepine from aqueous media: adsorption behavior and influential parameters. Arab. J. Chem. 9. https://doi.org/10.1016/j.arabjc.2016.12.025.
Nam, S.W., Choi, D.J., Kim, S.K., Her, N., Zoh, K.D., 2014. Adsorption characteristics of selected hydrophilic and hydrophobic micropollutants in water using activated carbon. J. Hazard Mater. 270, 144–152.
Namduri, H., Nasrazadani, S., 2008. Quantitative analysis of iron oxides using Fourier transform infrared spectrophotometry. Corros. Sci. 50, 2493–2497.
Ng'eno, E., Shikuku, V.O., Orata, F., Lilechi, D.B., Kimosop, S., 2019. Caffeine and Ciprofloxacin Adsorption from water onto clinoptilolite: linear isotherms, kinetics, thermodynamics and mechanistic studies. S. Afr. J. Chem. 72, 136–142.
Oetken, M., Nentwig, G., Loffler, D., Ternes, T., Oehlmann, J., 2005. Effects of pharmaceuticals on aquatic invertebrates. Part I. The antiepileptic drug carbamazepine. Arch. Environ. Contam. Toxicol. 49, 353–361.
Punyapalakul, P., Sitthisorn, T., 2010. Removal of ciprofloxazin and carbamazepine by adsorption on functionalized mesoporous silicates. World Academy Sci. Eng. Technol. 69, 546–550.
Rajendran, K., Sen, S., 2018. Adsorptive removal of carbamazepine using biosynthesized hematite nanoparticles. Environ. Nanotechnol. Monit. Manag. 122–127.
Saleh, T.A., 2015. Isotherm, kinetic, and thermodynamics studies on Hg(II) adsorption from aqueous solution by silica-multiwall carbon nanotubes. Environ. Sci. Pollut. Res. 22, 16721–16731.
Schaider, L.A., Ruthann, A.R., Ackerman, J.M., Dunagan, S.C., Brody, J.G., 2014. Pharmaceuticals, perfluorosurfactants and other organic wastewater compounds in public drinking water wells in a shallow sand and gravel aquifer. Sci. Total Environ. 468–469, 384–393.
Shikuku, V.O., Donato, F.F., Kowenje, C.O., Zanella, R., Prestes, O.D., 2015. A comparison of adsorption equilibrium, kinetics and thermodynamics of aqueous phase clomazone between Faujasite X and a Natural zeolite from Kenya. S. Afr. J. Chem. 68, 245–252.
Shikuku, V.O., Kowenje, C.O., Kengara, F., 2018b. Errors in parameters estimation using linearized adsorption isotherms: sulfadimethoxine adsorption onto kaolinite clay. Chem. Sci. Inter. J. 23 (4), 1–6.
Shikuku, V.O., Zanella, R., Kowenje, C.O., Donato, Filipe F., Bandeira, Nelson, Prestes, O.D., 2018a. Single and Binary Adsorption of sulphonamide antibiotics onto iron-modified clay: linear and nonlinear Isotherms, Kinetics, thermodynamics and mechanistic studies. Appl. Water Sci. 8, 175. https://doi.org/10.1007/s13201-018-0825-4.
Sosa, G., Morantes, C., Flores, F., Sánchez, R., Zalts, A., Ramirez, S., 2019. Characterization of diatomaceous earth modified by organic ligands for enhanced zinc adsorption. J. Environ. Chem. Eng. 7, 103197. https://doi.org/10.1016/j.jece.2019.103197.
Thacker, P.D., 2005. Pharmaceutical data elude researchers. Environ. Sci. Technol. 39, 193–194.
To, M., Hadi, P., Hui, C., Lin, C., McKay, G., 2017. Mechanistic study of atenolol, acebutolol and carbamazepine adsorption on waste biomass derived activated carbon. J. Mol. Liq. 241, 386–398.
Treybal, R.E., 1981. Mass-transfer Operations, 3rd ed., McGraw-Hill. using tree fern as a biosorbent. Process Biochem. 40 (1), 119–124.
Tsai, W., Lai, C., Ting-Yi, S., 2006. Adsorption of bisphenol-A from aqueous solution onto minerals and carbon adsorbents. J. Hazard Mater. 134, 169–175.
Volesky, B., 2007. Biosorption and me. Water Res. 41, 4017–4029.
Yu, W., Deng, L., Yuan, P., Liu, D., Yuan, W., 2015. Preparation of hierarchically porous diatomite/MFI-type zeolite composites and their performance for benzene adsorption : the effects of desilication. Chem. Eng. J. https://doi.org/10.1016/j.cej.2015.02.065.
Yuan, P., Liu, D., Tan, D., Liu, K., Yu, H., Zhong, Y., 2013. Microporous and Mesoporous Materials Surface silylation of mesoporous/macroporous diatomite (diatomaceous earth) and its function in Cu(II) adsorption : the effects of heating pretreatment. Microporous Mesoporous Mater. 170, 9–19. https://doi.org/10.1016/j.micromeso.2012.11.030.
Zhang, M., Gao, B., Varnoosfaderani, S., Hebard, A., Yao, Y., Inyang, M., 2013. Preparation and characterization of a novel magnetic biochar for arsenic removal. Bioresour. Technol. 130, 457–462. https://doi.org/10.1016/j.biortech.2012.11.132.
Zhang, Y., Geißen, S.U., Gal, C., 2008. Carbamazepine and diclofenac: removal in wastewater treatment plants and occurrence in water bodies. Chemosphere 73 (8), 1151–1161.
Zhao, Q., Zhang, S., Zhang, X., Lei, L., Ma, W., Ma, C., Song, L., Chen, J., Pan, B., Xing, B., 2017. Cation-Pi interaction: a key force for sorption of fluoroquinolone antibiotics on pyrogenic carbonaceous materials. Environ. Sci. Technol. 51, 13659–13667.
Zheng, L., Yang, Y., Meng, P., Peng, D., 2019. Absorption of cadmium (II) via sulfur-chelating based cellulose: Characterization, isotherm models and their error analysis. Carbohydr. Polymers 209, 38–50.